Catal Lett (2009) 130:147–153
DOI 10.1007/s10562-009-9840-2

Synthesis of $CaIn_2O_4$ Rods and Its Photocatalytic Performance Under Visible-light Irradiation

Jianjun Ding · Song Sun · Jun Bao · Zhenlin Luo · Chen Gao

Received: 4 October 2008 / Accepted: 1 January 2009 / Published online: 30 January 2009

Abstract A type of $CaIn_2O_4$ particle was synthesized at a relatively low temperature by a solution-combustion method using calcium nitrate and indium nitrate as oxidizers and glycine as a fuel, followed by a high-temperature postannealing, during which the nanometric grains of the as-combusted $CaIn_2O_4$ powder self-assembled into nano-capsules, and subsequently the nano-capsules linked end to end to form the regular $CaIn_2O_4$ rods with the diameter of 300 nm and the length of about 2 μm. The $CaIn_2O_4$ rods showed significantly higher photocatalytic activity for methylene blue degradation and toluene oxidation under visible-light irradiation than that of the sample synthesized by the conventional solid-state reaction. Particularly, the Pt-dispersed $CaIn_2O_4$ rods exhibited excellent photocatalytic activity for water decomposition under visible-light irradiation. The high crystallization degree, low impurity level and relatively large surface area of $CaIn_2O_4$ rods were considered as the important factors for its high photocatalytic performance.

Keywords $CaIn_2O_4$ rods · Solution-combustion method · Visible-light Photocatalysis

J. Ding · S. Sun · J. Bao (✉) · Z. Luo · C. Gao (✉)
National Synchrotron Radiation Lab, University of Science & Technology of China, 230029 Hefei, Anhui, People's Republic of China
e-mail: baoj@ustc.edu.cn

C. Gao
e-mail: cgao@ustc.edu.cn

C. Gao
Hefei National Laboratory for Physical Sciences at the Micorscale, University of Science & Technology of China, 230029, Hefei, Anhui, People's Republic of China

1 Introduction

The development of visible-light induced photocatalyst is of great importance for the efficient utilization of solar energy or indoor artificial light in the photocatalytic degradation of organic pollutants and splitting of water. Until now, most of the related studies have been focused on the modification of TiO_2, an ultraviolet (UV) light photocatalyst, to shift its absorption band into the visible range [1–3]. A few efforts have also been carried out on the development of new materials with intrinsic visible photocatalytic activity, represented by the recent significant work of Zou and Domen et al. [4–7] in which a series of new semiconductor oxides were developed to exhibit a strong photocatalytic effect on water splitting and organic contaminant degradation under the visible-light irradiation, such as $In_{0.9}Ni_{0.1}TaO_4$ and $(Ga_{1-x}Zn_x)(N_{1-x}O_x)$.

More recently, Inoue and Zou et al. have demonstrated that the p-block metal oxides of MIn_2O_4 (M = Ca, Sr, Ba) have good photocatalytic activity for degrading organic pollutants such as methylene blue (MB) under visible-light irradiation or splitting of water into hydrogen and oxygen by the dispersion of RuO_2 under the UV irradiation [8–14]. The p-block metal oxides are electronically composed of octahedrally coordinated metal ions with the d^{10} configuration. Among these oxides, the $CaIn_2O_4$ shows the highest photocatalytic activity because the material has the smallest radii of ion and similar InO_6 octahedra network structure, which is beneficial for the photoelectrons transfer. Solid-state reaction (SSR) is the conventional method widely used for preparing these materials, during which the oxides of the starting materials are mixed together followed by being calcined at high temperature for a sufficient length of time [15]. Due to the evaporation of In_2O_3 above 1,273 K [16], the SSR method is difficult to synthesize

pure phase $CaIn_2O_4$. Furthermore, the method does not mix various components at the molecular level so that the agglomeration may occur, which often producing an extremely low surface area and more lattice defects.

In order to provide fundamental understanding of the crystal chemistry of these materials and achieve improved properties, some researchers have attempted to prepare these materials using special processing techniques, such as the co-precipitation or combustion [11, 15], which are useful either in the reduction of the synthesis temperature or to better control over the particle size. Using the co-precipitation method Inoue et al. synthesized a kind of $CaIn_2O_4$ particles with better photocatalytic activity than that of the sample prepared by the SSR method [11]. Combustion synthesis was found to be successful in preparing many metastable phases and also conventional materials at low temperature [17]. Esther Dali et al. [15] prepared a kind of $CaIn_2O_4$ by a combustion method using the urea as fuel. However, the resulting $CaIn_2O_4$ was impure with a small amount of CaO and In_2O_3 still remaining after calcination at 1,323 K for 6 h. In the present study, a kind of pure $CaIn_2O_4$ particle was prepared at a relatively low temperature by a modified solution-combustion (SC) method. The following high-temperature treatment made the nanometric particles grow into regular $CaIn_2O_4$ rods. The obtained sample was characterized by XRD, TEM, BET, UV/Vis diffuse reflectance spectra and its photocatalytic performances for MB degradation, toluene oxidation and water decomposition under visible-light irradiation were investigated.

2 Experimental

2.1 Catalysts Preparation

$CaIn_2O_4$ sample was synthesized by the combustion of an aqueous redox mixture of stoichiometric amounts of calcium nitrate, indium nitrate and glycine, followed by a high temperature postannealing. The detailed procedure was as follows: 0.945 g $Ca(NO_3)_2 \cdot 4H_2O$, 3.055 g $In(NO_3)_3 \cdot 9/2H_2O$ and 1.334 g $C_2H_5NO_2$ were dissolved in 20 ml deionized water. The mixed solution was kept at 473 K for 30 min, and then slowly heated to 573 K in 30 min. During this period, a spontaneous combustion took place and a fluffy powder was formed. The chemical reaction in the combustion can be represented by the following equation:

$$Ca(NO_3)_2 + 2In(NO_3)_3 + \frac{40}{9}C_2H_5NO_2 = CaIn_2O_4 + \frac{100}{9}H_2O + \frac{80}{9}CO_2 + \frac{56}{9}N_2$$

The fluffer was annealed at 1,373 K for 12 h in air. An intermediate sample for TEM investigation was annealed at the same temperature for 2 h. For comparison, a $CaIn_2O_4$ sample was synthesized by the conventional SSR method as reported in literature [8–10, 18]. The sample was finally calcined at 1,373 K for 24 h in air.

2.2 Characterization Methods

X-ray diffraction (XRD) patterns were measured with a Rigaku D/max-γA rotation anode diffractometer with $Cu_{K\alpha}$ radiation ($\lambda = 0.15418$ nm). The BET surface area was determined by an adsorption method (Micromeritics ASAP 2000) with N_2 as the adsorbent. Transmission electron microscopy (TEM) images were taken on a HitachiH-800 TEM operating at 200 kV. The UV/Vis diffuse reflectance spectrum was measured on a UV/Vis spectrometer (SolidSpec-3700, Shimadzu, Japan).

2.3 Measurement of Photocatalytic Activity

The photocatalytic activity of the prepared $CaIn_2O_4$ for MB degradation, toluene oxidation and water decomposition under visible-light irradiation was investigated. For the MB degradation, 0.36 g $CaIn_2O_4$ synthesized either from SSR or SC methods (as combusted or annealed) was suspended in 120 ml MB solution with a concentration of 20.1 μmol L^{-1} in a Pyrex glass cell. The initial pH value of the solution was near 7. The optical system used for the photocatalytic reaction consisted of a 300 W Xe arc lamp (PLS-SXE300, ChangTuo Ltd, China), a wavelength-selective beamsplitter (infrared transmission, visible/UV reflection) and an UV cut-off filter. The effective output power of the Xe arc lamp is 47 W. The light of the lamp was first reflected by the beamsplitter, and then passed through the filter before entering the Pyrex glass cell. To eliminate the thermal effect, a water jacket was used to keep the solution's temperature constant at room temperature by flowing cooling water. Before the reaction, the prepared suspension was magnetically stirred for about 30 min in the dark to eliminate the adsorption effect. The concentration changes of MB were monitored by measuring the absorbance at $\lambda = 665$ nm with a portable fiber spectrometer (Model SD2000, Ocean Optics). The absorption spectrum of the solution before and after reaction was measured on a UV/Vis spectrometer (SolidSpec-3700, Shimadzu, Japan). The concentration of SO_4^{2-} anion, one of the main products of MB degradation, was measured by an ion chromatograph with a conductivity detector (IC1010, Techcomp).

The toluene oxidation and water splitting experiments were performed using a closed gas circulation system and

an outside-irradiation type reactor. The same optical system and water jacket mentioned above were employed. The photocatalytic decomposition of toluene was performed with 0.35 g of the photocatalyst powder placed at the bottom of a Petri dish inside the reactor; the reaction gas mixture consisted of 175 ppm toluene, 22% O_2 and N_2 balance gas and 23% relative humidity. The CO_2 and toluene concentrations in the effluent gas were measured with a gas chromatograph (Kexiao GC-1690) equipped with a thermal conductivity detector (TCD), a flame ionization detector (FID) and a methane converter. The splitting of water was carried out with 0.35 g photocatalyst powder suspended in 120 mL pure water of CH_3OH aqueous solution (CH_3OH: 20 mL; H_2O: 100 mL). The H_2 evolved was analyzed on a TCD gas chromatograph (Shimadzu GC-14C, TCD sensitivity $\geq$5,000 mV mL mg^{-1} (benzene), equipped with a carboxen 1000 column). The apparent quantum efficiency was measured using a band-pass filter ($\lambda = 420$ nm, half-width: 12 nm). The calculation equation is shown as follows:

$$\Phi(\%) = \frac{\text{No. of reacted electrons}}{\text{No. of indicent photons}} \times 100 = \frac{\text{No. of evolved } H_2 \text{ molecules} \times 2}{\text{No.of incident photons}} \times 100$$

Here, Φ is the apparent quantum efficiency, where it is assumed that all incident photons are absorbed by the photocatalyst.

3 Results and Discussion

The XRD patterns of the as-combusted fluffer, the post-annealed powder and the sample synthesized by the conventional SSR method are shown in Fig. 1. Basically, they showed almost the same diffraction peaks, all of which can be indexed into the orthorhombic phase of $CaIn_2O_4$ (PDF No. 17-0643). Further comparison showed that the XRD patterns of the as-combusted fluffer and the postannealed powder were smoother than that of the SSR method derived sample, indicating a better crystallization. The results showed that the pure phase of $CaIn_2O_4$ can be synthesized at a relatively low temperature by the modified SC method.

The microstructure of these samples was investigated using the TEM technique. As shown in Fig. 2a, the $CaIn_2O_4$ synthesized by the conventional SSR method had an irregular shape with size of $\sim$600 nm while the as-combusted $CaIn_2O_4$ fluffer showed a fine spherical shape with size of $\sim$90 nm (Fig. 2b). After calcination, the $CaIn_2O_4$ particles had a regular shape of rod, as shown in Fig. 2c. The average

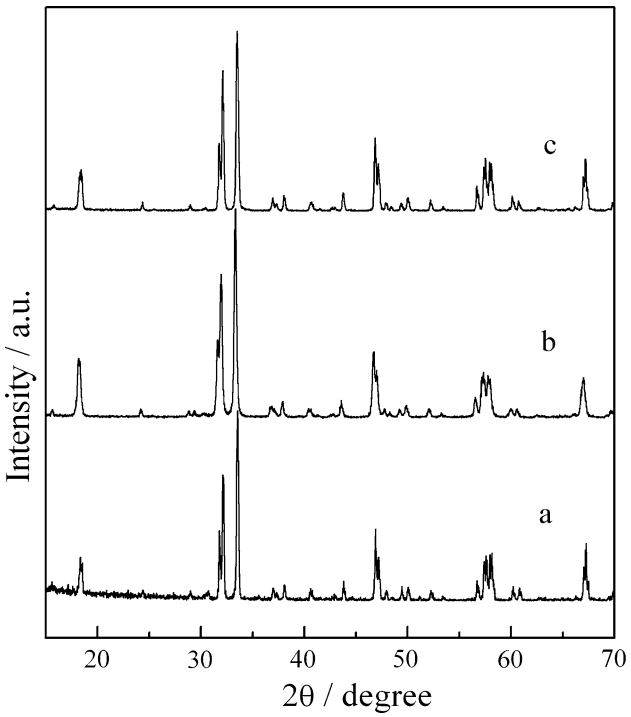

Fig. 1 XRD patterns of the samples. (*a*) synthesized by the SSR method; (*b*) as-combusted and (*c*) postannealed at 1,373 K for 12 h

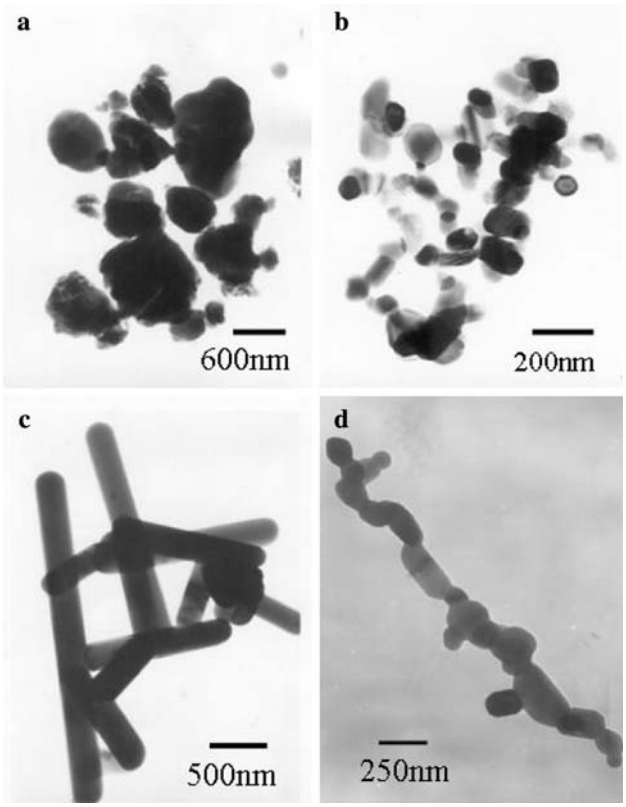

Fig. 2 TEM images of $CaIn_2O_4$. **a** synthesized by the SSR method; **b** as-combusted; **c** postannealed at 1,373 K for 12 h and **d** an intermediate in the postannealing (1,373 K for 2 h)

diameter and length of the rods was about 300 nm and 2 μm, respectively. To reveal the formation of the rods, TEM image of an intermediate that was postannealed at the same temperature for only 2 h was taken and shown in Fig. 2d. This image clearly demonstrated that the nanometric grains of the as-combusted fluffer self-assembled into nano-capsules first, then the nano-capsules linked end to end to form the final rods during the postannealing. Similar self-assembling behavior has been reported in solution synthesis but was rarely observed, to our best knowledge, in the postannealing of solid powders. The asymmetric crystal structure of $CaIn_2O_4$ and the instantaneous high temperature in the combustion may play an important role in the formation of the rods. Further studies are undergoing on the growth mechanism of the rods. The BET surface area of the SSR sample, the as-combusted $CaIn_2O_4$ fluffer, and the $CaIn_2O_4$ rods were 0.95, 10.9 and 2.14 $m^2\ g^{-1}$, respectively. The $CaIn_2O_4$ derived from SSR method had the lowest surface area. The as-combusted $CaIn_2O_4$ fluffer, as expected, showed the largest surface area. After high-temperature postannealing, the surface area of the obtained $CaIn_2O_4$ rods decreased significantly.

Figure 3 shows the UV/Vis diffuse reflectance spectra of the SSR derived $CaIn_2O_4$ powder, the as-combusted fluffer and the postannealed $CaIn_2O_4$ rods. The SSR derived $CaIn_2O_4$ had the similar absorption characteristics with that of the literature's sample prepared by the SSR or co-precipitation methods, in which two absorption edges were clearly identified [8, 11]. For the as-combusted $CaIn_2O_4$ fluffer, only a broad and smooth absorption band was observed in the region of 290–450 nm. After calcination, the absorption edge of $CaIn_2O_4$ rods became steeper. The steep absorption edge suggested that the $CaIn_2O_4$ rods had a low impurity level. Compared with the SSR derived sample, the absorption onset of $CaIn_2O_4$ rods shifted to shorter wavelength, which may be attributed to the quantum-size effect because of the smaller particle size [19].

The photocatalytic activities of the three kinds of $CaIn_2O_4$ for the MB degradation under visible-light irradiation were tested under the same conditions. Figure 4 shows the MB concentration as the function of visible-light irradiation time for the three photocatalysts. A dark experiment without light irradiation was carried out (not shown) and no degradation of MB was observed without light irradiation. The MB photolysis, namely without the photocatalyst, was also performed under the same conditions. It was obvious that the photolysis rate of MB was much lower than that of the MB degradation over the $CaIn_2O_4$ samples, proving that the prepared materials were active for MB photocatalytic degradation under visible-light irradiation. The as-combusted $CaIn_2O_4$ fluffer showed a higher activity than that of the $CaIn_2O_4$ derived from the SSR method. The $CaIn_2O_4$ rods, although their surface areas decreased remarkably, exhibited the best performance for MB degradation. It took only 90 min to decompose the MB dye in the solution under visible-light irradiation. The effects of calcination temperature and time on the photocatalytic activities of the SC method derived $CaIn_2O_4$ were investigated. Figures 5 and 6 show the MB concentration of the solution after 90 min irradiation on the $CaIn_2O_4$ with different calcination temperature and time,

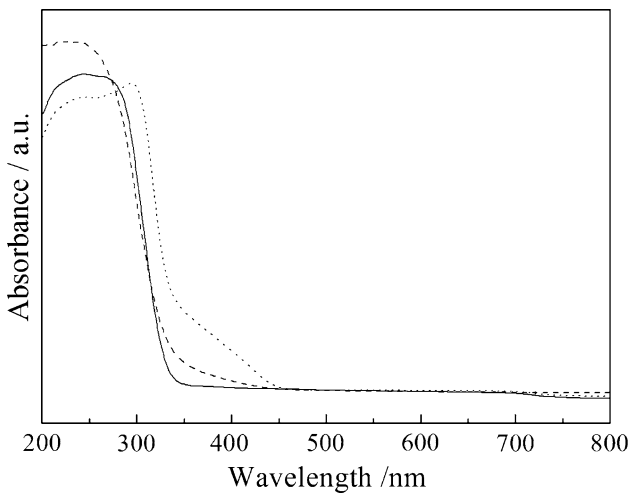

Fig. 3 UV/Vis diffuse reflectance spectra of the SSR derived $CaIn_2O_4$ powder (*dotted line*), the as-combusted fluffer (*dash line*) and the postannealed $CaIn_2O_4$ rods (*solid line*)

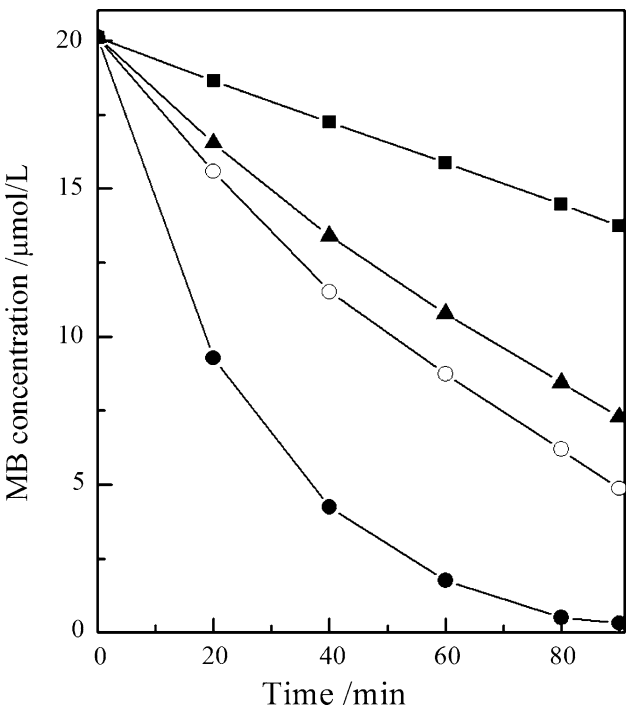

Fig. 4 Concentration of MB dye as functions of the visible light irradiation time. (■) MB photolysis; (▲) synthesized by the SSR method; (○) as-combusted $CaIn_2O_4$ and (●) $CaIn_2O_4$ rods

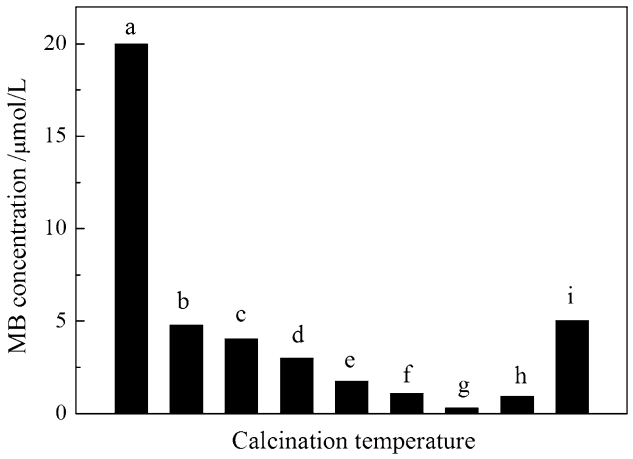

Fig. 5 MB concentration of the solution after 90 min irradiation on the $CaIn_2O_4$ calcined at different temperature. (*a*) original solution; (*b*) as-combusted fluffer; (*c*) 973 K for 12 h; (*d*) 1,073 K for 12 h; (*e*) 1,173 K for 12 h; (*f*) 1,273 K for 12 h; (*g*) 1,373 K for 12 h; (*h*) 1,473 K for 12 h; (*i*) 1,573 K for 12 h

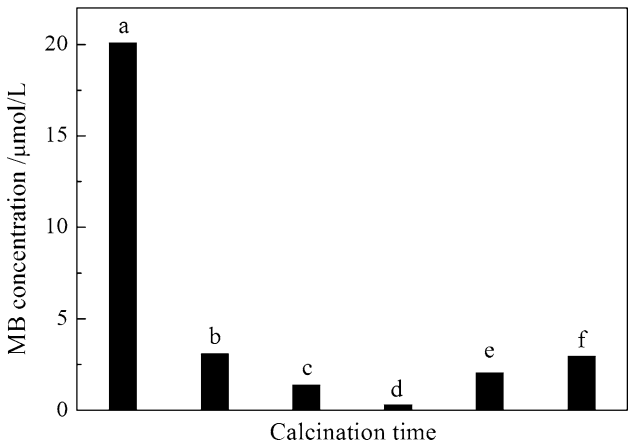

Fig. 6 MB concentration of the solution after 90 min irradiation on the $CaIn_2O_4$ calcined at 1,373 K with different time. (*a*) original solution; (*b*) 1,373 K for 2 h; (*c*) 1,373 K for 6 h; (*d*) 1,373 K for 12 h; (*e*) 1,373 K for 24 h; (*f*) 1,373 K for 48 h

respectively. It can be seen that when increasing the calcination temperature or time, the photocatalytic activities of the $CaIn_2O_4$ for MB degradation increased initially, followed by a rapid decrease. The optimal calcination conditions were 1,373 K for 12 h. The results can be attributed to the joint effect of surface area and crystallization of particles [11]. The high-temperature treatment produced a low surface area, but meanwhile, through crystallization, eliminated the impurities and structural imperfections that act as recombination sites for photoexcited charges. The absorbances of the MB solution before and after the photocatalytic reaction of $CaIn_2O_4$ rods were analyzed by a UV/Vis spectrometer. As shown in Fig. 7, all the absorption peaks of MB disappeared and no new peak was observed in the solution after reaction, indicating that

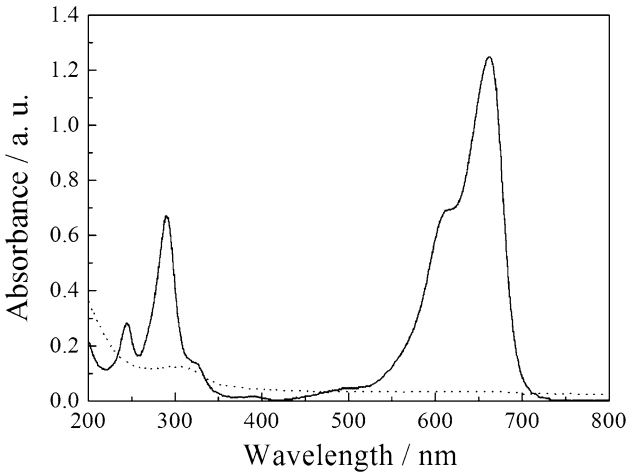

Fig. 7 The absorption spectra of MB solution before (*solid line*) and after the photocatalytic reaction (*dotted line*)

the aromatic rings and conjugated π-system in MB did not exist [8]. The solutions before and after the photocatalytic reaction of $CaIn_2O_4$ rods were also analyzed using the ion chromatography. The concentration of SO_4^{2-} anion, one of the main mineralization products of MB degradation, was detected to be 0 and 9.65 μmol L^{-1} in the solution before and after the photocatalytic reaction, respectively. This result indicates that 48% of the sulfur in MB was converted into sulfate, which is in good agreement with the result reported in references [8, 20]. These findings clarify that the MB was decomposed rather than absorbed over the $CaIn_2O_4$ rods under visible-light irradiation. Subsequently, the $CaIn_2O_4$ photocatalysts were employed to decompose the gaseous toluene under visible-light irradiation. During the photocatalytic degradation, toluene was first oxidized to intermediate compounds such as benzaldehyde and benzoic acid, which was further decomposed to become final products CO_2 and H_2O [21, 22]. In the present study, the toluene removal ratio and mineralization ratio of three kinds of $CaIn_2O_4$ photocatalysts were measured and presented in Fig. 8. The $CaIn_2O_4$ rods showed much higher activity than other two samples. Its toluene removal ratio and mineralization ratio were 74 and 66%, respectively, more than four times than that of the SSR derived sample. The discrepancy between the removal ratio and mineralization ratio is due to the fact that some of the reaction intermediates are stable and hardly oxidized compared with toluene [23].

The water decomposition on the synthesized $CaIn_2O_4$ rods under visible-light irradiation was also measured. Previous studies have demonstrated that the $CaIn_2O_4$ combined with RuO_2 can split water under UV irradiation [11, 14]. In the present study, the Pt was used as the promoter to modify the $CaIn_2O_4$ and the photocatalytic activity for water decomposition under visible-light

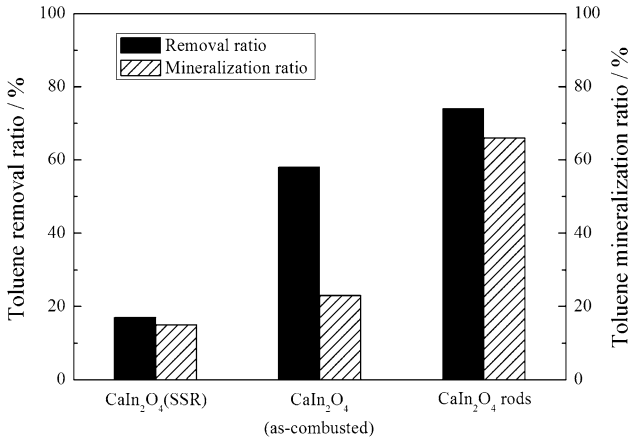

Fig. 8 Removal ratio and mineralization ratio of the toluene after 360 min irradiation on the $CaIn_2O_4$

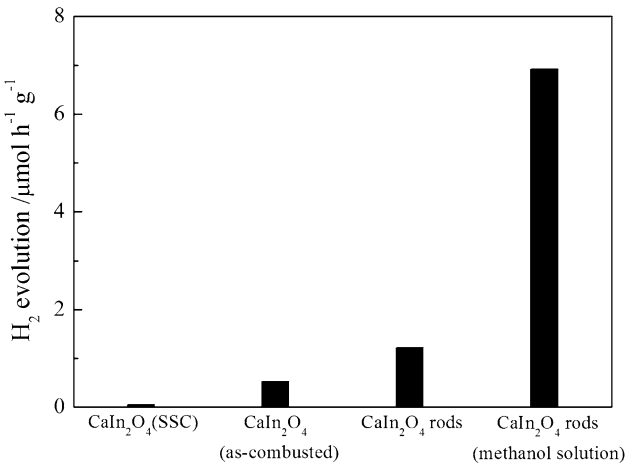

Fig. 9 Photocatalytic activities of 0.5 wt% Pt-dispersed $CaIn_2O_4$ catalysts for water decomposition under visible-light irradiation

irradiation was investigated. The Pt-dispersed $CaIn_2O_4$ was prepared by an incipient impregnation method using chloroplatinic acid as metal precursor. After impregnation, the sample was dried at 383 K for 24 h, and then reduced at 573 K in pure H_2 flow for 2 h. Figure 9 shows the photocatalytic activities of 0.5 wt% Pt/$CaIn_2O_4$ catalysts for water decomposition under visible-light irradiation. The combustion derived catalysts, especially the $CaIn_2O_4$ rods, exhibited excellent activity for water decomposition with the dispersion of Pt. The formation rate of H_2 evolution over the Pt-dispersed $CaIn_2O_4$ rods were 1.23 μmol $h^{-1}g_{cat}^{-1}$, approximately 24 times higher than that of the SSR derived $CaIn_2O_4$. The presence of methanol further increased the H_2 production rate up to 6.92 μmol $h^{-1}g_{cat}^{-1}$. The changes in the photocatalytic activity with the amount of Pt dispersed on $CaIn_2O_4$ rods are presented in Fig. 10. In the absence of Pt, the photocatalytic activity was negligible. The addition of Pt significantly promoted the H_2 production. The activity increased with increasing the Pt loading and reached the

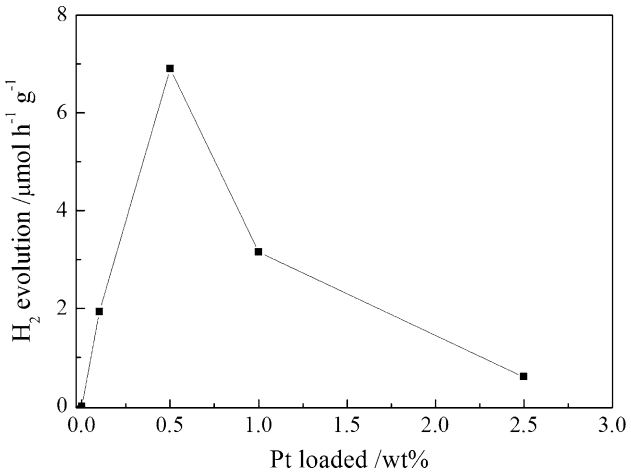

Fig. 10 Photocatalytic activities of Pt-dispersed $CaIn_2O_4$ rods as a function of Pt amount

maximum at Pt loading of 0.5 wt%. Further increase resulted in a remarkable activity fall. The apparent quantum efficiency for H_2 evolution over the 0.5 wt% Pt/$CaIn_2O_4$ rods was estimated to be ca. 0.24%. The $CaIn_2O_4$ rods were recycled two times in the above photocatalytic reactions and no significant loss of activity was observed. The crystal structure and color of the photocatalyst also did not change after reactions. These results indicated that the $CaIn_2O_4$ rods synthesized by SC method were a stable and effective photocatalyst.

Zou and Ye et al. [9] investigated a series of MIn_2O_4 (M = Ca, Sr, Ba) visible-light response photocatalysts and found that the $CaIn_2O_4$ showed the highest activity although its light absorption ability was weak. The reason was that the $CaIn_2O_4$ had excellent photoelectrons transfer ability due to its distorted InO_6 octahedra structure. Sato and Inoue et al. [12] reported the distorted InO_6 octahedra had a significant dipole moment which can promote the charge separation. The materials composed of the uniform InO_6 octahedra network are beneficial to the charge transfer to surface of the materials. Furthermore, the same authors reported that the well-crystallized $CaIn_2O_4$ led to high photocatalytic performance due to the elimination, through crystallization, of impurities and structural imperfections that act as recombination sites for photoexcited charges [11]. For the presented $CaIn_2O_4$ photocatalyst, the regular rod shape of particles, as well as the XRD and diffuse reflectance spectra results, demonstrated that the synthesized $CaIn_2O_4$ had a high crystallization degree and low impurity level, which can decrease the recombination probability of photoexcited electron and hole and improve the charge transfer ability to the surface of the photocatalyst. Beside that, the relatively large surface area of $CaIn_2O_4$ rods was also the important factor for its high photocatalytic activity. Further studies on electronic and crystal structures of the $CaIn_2O_4$ rods are in progress and will be reported elsewhere.

4 Conclusion

In this study, a solution-combustion method was developed to prepare a kind of $CaIn_2O_4$ nano-particle at low temperature followed by a high-temperature treatment which made the nanometric particle grow into regular $CaIn_2O_4$ rods with the diameter of 300 nm and length of 2 μm through a self-assembling behavior. Due to the high crystallization, low impurity level and large surface area, the $CaIn_2O_4$ rods showed significantly higher photocatalytic activity for MB degradation and toluene oxidation under visible-light irradiation compared with the sample synthesized by the conventional SSR method. Furthermore, with the dispersion of Pt, the $CaIn_2O_4$ rods exhibited an excellent photocatalytic activity for water decomposition under visible-light irradiation.

Acknowledgments This work was supported by NSFC (grant#: 50721061).

References

1. Asahi R, Ohwaki T, Aoki K, Taga Y (2001) Science 293:269–271
2. Kisch H, Zang L, Lange C, Maier WF, Antonius C, Meissner D (1998) Angew Chem 110:3201–3203
3. Anpo M, Takeuchi M (2003) J Catal 216:505–516
4. Zou ZG, Ye JH, Sayama K, Arakawa H (2001) Nature 414:625–627
5. Tang JW, Zou ZG, Ye JH (2004) Angew Chem Int Ed 43:4463–4466
6. Maeda K, Takata T, Hara M, Saito N, Inoue Y, Kobayashi H, Domen K (2005) J Am Chem Soc 127:8286–8287
7. Lu DL, Takata T, Saito N, Inoue Y, Domen K (2006) Nature 440:295
8. Tang JW, Zou ZG, Ye JH (2003) Chem Phys Lett 382:175–179
9. Tang JW, Zou ZG, Katagiri M, Kako T, Ye JH (2004) Catal Today 93–95:885–889
10. Tang JW, Zou ZG, Ye JH (2004) Chem Mater 16:1644–1649
11. Sato J, Saito N, Nishiyama H, Inoue Y (2003) J Phys Chem B 107:7965–7969
12. Sato J, Kobayashi H, Inoue Y (2003) J Phys Chem B 107:7970–7975
13. Sato J, Saito N, Nishiyama H, Inoue Y (2001) Chem Lett 30:868–869
14. Sato J, Saito N, Nishiyama H, Inoue Y (2001) J Phys Chem B 105:6061–6063
15. Esther Dali S, Sai Sundar VVSS, Jayachandran M, Chockalingam MJ (1998) J Mater Sci Lett 17:619–623
16. Weast RC, Lide DR, Astle MJ, Beyer WH (eds) (1989–1990) Handbook of chemistry and physics, 7th edn, CRC Press, Boca Raton
17. Kingsley JJ, Patil KC (1988) Mater Lett 6:427–432
18. Cruickshank FR, Taylor McKD, Glasser FP (1964) J Inorg Nucl Chem 26:937
19. Hoffman AJ, Yee H, Mills G, Hoffmann MR (1992) J Phys Chem 96:5540–5546
20. Qu P, Zhao JC, Shen T, Hidaka H (1998) J Mol Catal A 129:257–268
21. Cao LX, Gao Z, Suib SL, Obee TN, Hay SO, Freihaut JD (2000) J Catal 196:253–261
22. D'Hennezel O, Pichat P, Ollis DF (1998) J Photochem Photobiol A 118:197–204
23. Inaba R, Fukahori T, Hamamoto M, Ohno T (2006) J Mol Catal A Chem 260:247–254